Nonlinear Dyn (2021) 104:1475–1489
https://doi.org/10.1007/s11071-021-06318-1

ORIGINAL PAPER

Functional brain network dynamics based on the Hindmarsh–Rose model

Guiyang Lv · Nayue Zhang · Kexin Ma · Jian Weng · Ping Zhu · Feiyan Chen · Guoguang He

Received: 22 October 2020 / Accepted: 20 February 2021 / Published online: 7 March 2021

Abstract In order to reveal the dynamics of brain network, we proposed a new research method based on the Hindmarsh–Rose model. In the method, a neural network model was developed by constructing a functional brain network topology based on functional magnetic resonance imaging resting-state data and using Hindmarsh–Rose neurons as nodes in place of the brain regions belonging to the functional brain network. The dynamics of the functional brain network were investigated using the dynamics model. The simulation results showed that the dynamic behaviors of the brain regions in the functional brain network could be divided into three types: stable, chaotic, and periodical bursts. A state space was introduced to analyze the dynamic behavior of the brain regions in the network. We find that increasing excitation and mutual connection strength among brain regions enhanced network communication capabilities in the state space. Both the periodic and stable modes exhibited stronger communication capabilities than the chaotic mode. Despite individual differences in the dynamics of brain regions among subjects, brain regions in the periodic mode were highly consistent and corresponded to key regions of the default mode network in the resting state.

Keywords Brain dynamics · Functional brain networks · Hindmarsh–Rose model · Default mode networks

G. Lv · N. Zhang · K. Ma · P. Zhu · F. Chen · G. He (✉)
Department of Physics, Zhejiang University, Hangzhou 310027, People's Republic of China
e-mail: gghe@zju.edu.cn

J. Weng
Center of Brain Imaging Science and Technology, Key Laboratory for Biomedical Engineering of Ministry of Education, College of Biomedical Engineering and Instrumental Science, Zhejiang University, Hangzhou 310027, People's Republic of China

1 Introduction

Understanding human brain dynamics is of great significance for developing artificial intelligence [1–5] and treating neurological diseases such as Alzheimer's disease (AD) and schizophrenia [6]. Current research on brain dynamics is mainly conducted at the micro- and macro-levels. Micro-level investigations are focused on exploring the dynamic characteristics of individual neurons or neural circuits at the cellular and molecular levels, whereas electroencephalography (EEG), functional magnetic resonance imaging (fMRI), and other live-imaging technologies are used to reveal the relationship between neuronal populations and their advanced activities with related brain functions [7].

Since neurons are the most basic unit of neural systems, their spontaneous activity and interaction with other neurons are the basis of brain information transmission and information processing. In view of the importance of neuron dynamics, many single-neuron models were proposed in the twentieth century. In 1952, Hodgkin and Huxley proposed the Hodgkin–Huxley model (H–H model) based on experimental

data from the squid giant axon [8], which provides a mechanistic description for the generation of membrane action potentials when ions enter and exit neuronal cells. However, the H–H model is relatively complex and has a high computational cost. Thus, it is not suitable for large-scale calculations. FitzHugh and Nagumo simplified the H–H model and proposed a phenomenological FHN model [9,10]. Another similar model is the Rössler oscillator [11,12]. The above two models can be described using relatively simple equations for generating spikes and have low computational cost; however, they cannot imitate all behaviors of biological neurons. Hindmarsh and Rose proposed the Hindmarsh–Rose (HR) neuron model based on the discharge data of snail nerve cells [13]. The HR model is a universal model that can capture the essential dynamics observed in single neurons, groups of neurons, and brain areas [7]. The HR model not only generates periodic and chaotic spikes as singletons, but also bursts of spikes in periodic and chaotic ways. Some neurons produce different dynamic behaviors in external variables, such as electromagnetic field and temperature. Based on these phenomena, a thermosensitive neuron model is proposed. Recently, Xu et al. investigated the dynamic behavior of a thermosensitive neuron driven by temperature and photocurrent [14,15]. Compared with other neuron models, the HR model shows more abundant dynamic phenomena, and can imitate several behaviors of the thalamic nerve and reproduce some behaviors of the neuron population [7]. In addition, it saves computational time.

Owing to the limitations of current technology, it is difficult to determine the interaction between neurons in the brain with direct experimental measurements, but one can simulate the interaction between neurons by establishing a neural network coupled with neuron models. There are many dynamic studies on neural networks based on single-neuron models, such as synchronous behavior among neurons in networks [16]. Hizanidis et al. found chimeric states in coupled HR neurons [17]. These dynamic behaviors have been observed in the brain activity of aquatic mammals and birds [18]. Malik et al. studied the synchronization among coupled HR neurons and successfully encoded and decoded neural signals using an HR neural network [19]. These dynamics studies based on simple structure networks with the HR model confirmed certain dynamic characteristics of neuron populations. Unfortunately, information on functional connectivity of real brain regions is lacking in these studies. Thus, the dynamic state of brain regions cannot correspond to real brain functional activities.

On the other hand, with the development of noninvasive imaging technologies, such as EEG, fMRI, and positron emission tomography (PET), functional connections between brain regions can be obtained, and a functional brain network can be developed. A small-world characteristic in functional brain networks, or the existence of a high degree of clustering and a short path between all elements, has been noted [20]. Therefore, the human brain can effectively organize and transmit internal and external information between multiple brain regions to achieve collaboration between different brain regions. Neurological diseases, such as AD and schizophrenia, are related to changes in functional connections between brain regions. Several research groups have reported that the functional brain networks of patients with AD show a loss of small-world properties with a significantly lower degree of clustering [21]. Noninvasive measurements revealed that the functional brain networks of patients with schizophrenia exhibit a decreased connectivity both at rest and at work compared with those of healthy controls; that is, the disruption of small-world characteristics in the functional brain networks of such patients [22,23]. Therefore, the topology of connections between brain regions is very important for proper brain function.

Building a neural network with a brain network connection structure and neuron dynamics has become a popular method for studying brain dynamics. Santos et al. built the brain structure network of a cat with HR neurons as nodes and obtained chimera-like states in a dynamic network model [24]. Kang et al. used diffusion spectrum imaging (DSI) data to construct a network model with a human brain connection structure based on the FHN model and analyzed synchronization and chimera states [25]. Pariz et al. [26] explored information transmission in a network. Ziaeemehr et al. studied the impact of delays on the collective dynamics of brain networks with a modular structure [27]. However, above dynamic behavior of the structural network does not correspond to actual brain function. The human brain selectively stimulates certain regions according to different tasks, whereas there may be no structural connection between these brain regions, an effect that can be measured by fMRI. The low-frequency oscillations of resting fMRI signals are related to spontaneous neuronal activity and have clear physiologi-

cal and pathological significance [28]. Functional connectivity reflects the correlation between brain regions when fMRI signals are measured. Some brain regions that are not directly connected in a structure may be correlated with each other in function [29]. The functional brain network is flexible and changes under different conditions. However, structural networks cannot reflect this information. Functional networks can more directly reflect the interactions between brain regions under different conditions. Therefore, It is a better way to introduce functional brain network structures in the study of brain dynamics.

To explore the dynamic behavior of brain regions in the human brain, we established a brain neurodynamic model with an HR model and a functional brain network constructed using fMRI data in the resting state. The human brain exhibits chaotic dynamics and rapid switching between chaotic and periodic states during advanced neural activities. Therefore, neurons in the brain may also have rich dynamic characteristics. In view of the advantages of HR neurons in describing the rich dynamic behaviors of neural systems and their relatively concise mathematical expressions, in this study, we aimed to construct a neural network using HR neuron as a node in place of a brain region. By studying the dynamics of brain regions, the dynamic behavior of the whole functional brain network in the resting state was revealed. To analyze the characteristics of different dynamic modes of brain regions, a two-dimensional state space composed of the burst time width and the number of spikes in the burst was introduced [30].

The remainder of this paper is organized as follows. The method of constructing functional brain networks in the resting state is introduced in Sect. 2. The characteristics of HR neurons and the dynamic model of functional brain networks are described in Sect. 3. Section 4 investigates the dynamic characteristics of functional brain networks. The similarities and differences between the different subjects were compared. Section 5 discusses our results using the default mode network (DMN). The conclusions are presented in the last section.

2 Topological structure of a functional brain network in the resting state

The functional brain network in this study was constructed based on fMRI resting-state data. As a commonly used nondestructive method in neuroscience, fMRI detects neuronal activity by recording blood oxygenation level-dependent signals, caused by changes in oxygenated and deoxygenated proteins in the blood. In this study, whole-brain fMRI data from 15 subjects were collected in the resting state. Subjects were instructed to keep their eyes closed, relax their minds, and remain as still as possible during data acquisition. We used anatomical automatic labeling as proposed by the Montreal Neurological Institute (MNI) to divide the brain into 90 regions, as shown in Table 1. After performing noise removal and position correction on the fMRI data, we calculated the Pearson correlation according to Eq. (1), where X_i and X_j are fMRI signals of the i-th and j-th brain regions, respectively. T represents the lengths of X_i and X_j and is equal to 180 here. $\overline{X_\mathrm{i}}$ and $\overline{X_\mathrm{j}}$ are the average values of X_i and X_j, respectively. The Pearson correlation is the most popular method for calculating the correlation coefficients of brain regions. Figure 1 shows the correlation matrix (90×90) among the brain regions of subject No. 9. Ordinate and abscissa correspond to a serial number of brain regions, and the correlation coefficients are shown by color bars.

$$R_{\mathrm{ij}} = \frac{\sum_{t=1}^{T} \left(X_\mathrm{i}(t) - \overline{X_i}\right)\left(X_\mathrm{j}(t) - \overline{X_\mathrm{j}}\right)}{\sqrt{\sum_{t=1}^{T} \left(X_\mathrm{i}(t) - \overline{X_\mathrm{i}}\right)^2}\sqrt{\sum_{t=1}^{T} \left(X_\mathrm{j}(t) - \overline{X_j}\right)^2}}. \tag{1}$$

When determining whether two brain regions are connected according to correlation strength, a threshold of the Pearson correlation should be introduced to eliminate the interference of experimental noise while at the same time maintaining a proper connection density between the brain regions of functional brain networks. The threshold value is usually based on the criterion that the connection density of functional brain networks is approximately 20%, and there is no isolated brain region in the network. By analyzing the connection matrices from the fMRI data of 15 subjects, we chose the threshold of the correlation coefficient to be 0.36. If the absolute value of the correlation coefficient between any two brain regions is greater than 0.36, a connection between the two brain regions exists, and the connection coefficient is 1. Otherwise, there is no connection between these two brain regions and the connection coefficient is 0. The Pearson correlation matrix was then changed to a connection matrix

Table 1 Regions of interest included in the AAL-atlas (45 in each cerebral hemisphere, 90 in total, odd/even numerical order for left/right hemisphere)

Number	Region	Abbreviation	Number	Region	Abbreviation
1,2	Amygdala	AMYG	47,48	Middle occipital gyrus	MOG
3,4	Angular gyrus	ANG	49,50	Superior occipital gyrus	SOG
5,6	Calcarine cortex	CAL	51,52	Olfactory	OLF
7,8	Caudate	CAU	53,54	Pallidum	PAL
9,10	Anterior cingulate gyrus	ACG	55,56	Paracentral lobule	PCL
11,12	Median cingulate gyrus	DCG	57,58	Parahippocampal cortex	PHC
13,14	Posterior cingulate cortex	PCC	59,60	Inferior parietal lobule	IPL
15,16	Cuneus	CUN	61,62	Superior parietal gyrus	SPG
17,18	Inferior frontal gyrus (opercular)	IFGoperc	63,64	Postcentral gyrus	PoCG
19,20	Orbitofrontal cortex (inferior)	ORBinf	65,66	Precentral gyrus	PreCG
21,22	Inferior frontal gyrus (triangular)	IFGtriang	67,68	Precuneus	PCUN
23,24	Superior frontal cortex (medial orbital)	ORBsupmed	69,70	Putamen	PUT
25,26	Middle frontal gyrus	MFG	71,72	Rectus gyrus	REC
27,28	Orbitofrontal cortex (middle)	ORBmid	73,74	Rolandic operculum	ROL
29,30	Superior frontal gyrus (dorsal)	SFGdor	75,76	Supplementary motor area	SMA
31,32	Superior frontal gyrus (medial)	SFGmed	77,78	Supramarginal gyrus	SMG
33,34	Orbitofrontal cortex (superior)	ORBsup	79,80	Inferior temporal gyrus	ITG
35,36	Fusiform gyrus	FFG	81,82	Middle temporal gyrus	MTG
37,38	Heschl gyrus	HES	83,84	Temporal pole (middle)	TPOmid
39,40	Hippocampus	HIP	85,86	Temporal pole (superior)	TPOsup
41,42	Insula	INS	87,88	Superior temporal gyrus	STG
43,44	Lingual gyrus	LING	89,90	Thalamus	THA
45,46	Inferior occipital gyrus	IOG			

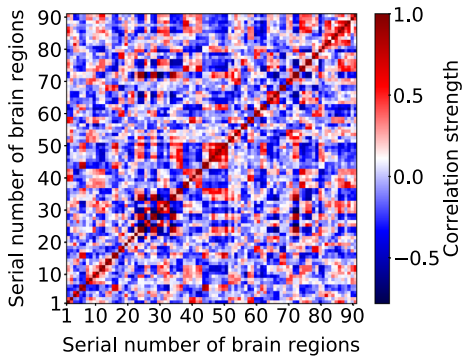

Fig. 1 Correlation coefficients of brain regions. Colors indicate the correlation strength between two brain regions

according to Eq. (2)

$$C_{ij} = \begin{cases} 0 & if \left|R_{ij}\right| < 0.36 \\ 1 & if \left|R_{ij}\right| \geq 0.36 \end{cases}, \tag{2}$$

where C_{ij} is the connection coefficient between the i-th brain region and the j-th brain region, and R_{ij} is the correlation coefficient between the i-th brain region and the j-th brain region.

Functional brain networks in the resting state can be obtained on the basis of the connection matrix C. The i-th brain region is connected to the j-th brain region if C_{ij} is 1. Otherwise, the two brain regions are not connected. The topological structure of the functional brain network for subject No. 9 is shown in Fig. 2.

A dynamic model of functional brain networks should be developed to investigate the dynamics of functional brain networks. Considering the chaotic dynamics of the nervous system and the advantages of the HR neuron, we introduced the HR model into the functional brain network and proposed a method to establish a corresponding dynamic model of brain networks, in which an HR neuron replaced a brain region

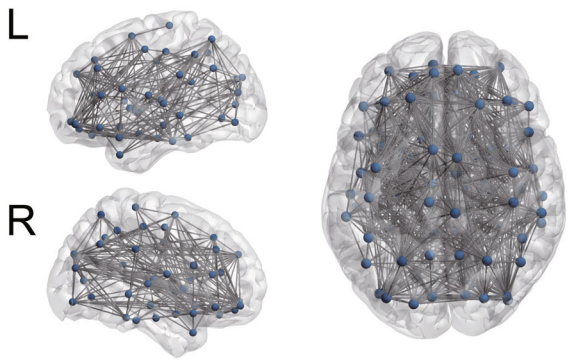

Fig. 2 Network topology of subject No. 9 (lateral and axial views). The functional brain network connection structure diagram after threshold processing. Nodes represent corresponding brain regions and are connected by a straight line if there is a connection between the two brains. The figure is plotted with BrainNet Viewer [31]

to construct the dynamic model of a functional brain network.

3 Functional brain network model based on HR neural network

3.1 HR neuron model

For the HR model, the dynamics of a neuron are determined using Eq. (3)

$$\begin{aligned} \dot{x} &= y - ax^3 + bx^2 - z + I_{bias} \\ \dot{y} &= c - dx^2 - y \\ \dot{z} &= r[s(x - x_{\mathrm{r}}) - z] \end{aligned} \quad , \tag{3}$$

where x represents the neuron membrane potential, y describes the fast current, z is the slow current, I_{bias} is the bias current that maintains the spontaneous activities of the neuron, and a, b, c, d, r, s, and x_{r} are parameters. The dynamics of an HR neuron are affected by parameter settings.

We take these parameters as $a = 1.0$, $b = 3.0$, $c = 1.0$, $d = 5.0$, $s = 4.0$, $r = 0.006$, $x_r = -1.56$. The initial values of x, y, and z are randomly generated between 0 and 1. Figure 3 shows three typical dynamic states of an HR neuron with I_{bias} set to 1.2, 1.6, and 2.9. The periodic single-pulse discharge in Fig. 3a corresponds to an I_{bias} of 1.2. Figure 3b shows stable bursts with the same spikes when I_{bias} is 1.6. As I_{bias} increases, chaotic bursts with different spikes appear, and the state of the HR neuron with I_{bias} of 2.9 is shown

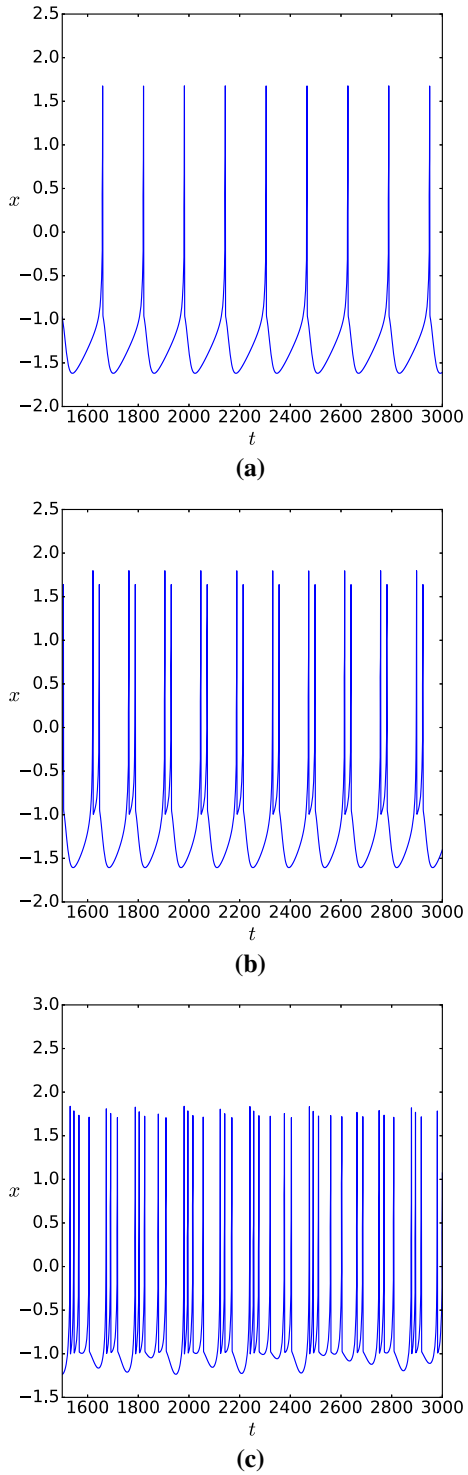

Fig. 3 Neuron membrane potential x. **a** $I_{\mathrm{bias}} = 1.2$, single-spike continuous periodic discharge. **b** $I_{\mathrm{bias}} = 1.6$, stable bursts with the same spikes. **c** $I_{\mathrm{bias}} = 2.9$, chaotic bursts with different spikes

in Fig. 3c. It can be observed from Fig. 3 that different I_{bias} values can change the dynamic characteristics of HR neurons and make HR neurons exhibit rich dynamic characteristics.

3.2 Functional brain network dynamics model

The topological structure of a functional brain network only exhibits a connection between brain regions and does not include information about the interaction strength between brain regions. The synapse weight should be determined as a neural network in response to a functional brain network. Since the correlation coefficient from fMRI data reflects the strength of cooperation between any possible brain region pair, a strong correlation implies close information transmission on activities in related brain regions. Therefore, the synapse weights of the neural network, representing the strength of information transmission between two neurons, can be defined by the Pearson correlation coefficients among brain regions. In this way, an HR neural network with 90 nodes is constructed to simulate the dynamics of functional brain networks, as described by Eq. (4) [17]

$$\begin{aligned} \dot{x}_{\text{i}} &= y_{\text{i}} - a x_{\text{i}}^3 + b x_{\text{i}}^2 - z_{\text{i}} + I_{\text{bias}} + \frac{\sigma}{90} \sum_{j=1}^{90} W_{ij} x_j \\ \dot{y}_{\text{i}} &= c - d x_{\text{i}}^2 - y_{\text{i}} + \frac{\sigma}{90} \sum_{j=1}^{90} W_{ij} y_j \\ \dot{z}_i &= r\,[s(x_{\text{i}} - x_{\text{r}}) - z_{\text{i}}] \end{aligned}, \tag{4}$$

where W_{ij} is the synapse weight of the network and $W_{ij} = C_{\text{i}j} R_{ij}$. Unlike a single neuron, x_{i} represents the spontaneous signal of the i-th brain region related to the self-interaction between brain regions. Owing to the magnitude difference between the correlation coefficients and the synapse weights, a gain factor σ is introduced in Eq. (4).

4 Dynamic characteristics of functional brain networks

4.1 Dynamic characteristics of an individual functional brain network

First, we investigated the dynamics of an individual functional brain network. Subject No. 9 was selected randomly as an example of the analysis. The parameters in the network described by Eq. (4) were the same as those of the HR model in 3.1. That is, $a = 1.0$, $b = 3.0$, $c = 1.0$, $d = 5.0$, $s = 4.0$, $r = 0.006$, $x_r = -1.56$, while both the gain factor σ and I_{bias} were taken to be 1.2. The fourth-order Runge–Kutta method was used to solve the differential equations. The step length was taken as 0.05, and the simulation range lasted from 0 to 50000. The initial values of x, y, and z were randomly set between 0 and 1.

An HR neuron with an I_{bias} of 1.2 shows the periodic single-pulse discharge in Fig. 3a, but all regions in the functional brain network with the same parameters are converted into bursts of spikes, as shown in Fig. 4. The parameters of the nodes are the same, but there are differences in the bursts of nodes owing to the functional brain network connection structure, as shown in Fig. 4a–f. It can be observed that the burst frequency is not the same for different brain regions. The spike number in one burst is obviously variable for some brain regions shown in Fig. 4a–f, whereas the spike number in one burst appears stable for other brain regions shown in Fig. 4b–d. This reveals that the dynamic behaviors of the different nodes are different.

To distinguish the dynamic properties of different brain regions, we counted the number of spikes in their bursts. As shown in Fig. 5, we identified three burst types. In Fig. 5a, the spike numbers of bursts remain constant, as in the right angular gyrus (ANG, R). In Fig. 5b, the spike numbers of bursts appear non-periodic, as in the left inferior frontal gyrus (triangular) (IFGtriang, L). Figure 5c illustrates quasi-periodic spike numbers, as in the left cuneus (CUN, L). Next, we used a spatial transformation to analyze the burst periodicity. The spike number of the n-th burst of one brain region is M_n, and the total number of bursts in the time range of [0, 50000] is N. The spatial transformation is defined as:

$$F[k] = \left| \sum_{n=0}^{N-1} M_n e^{-i2\pi kn/N} \right| / N. \tag{5}$$

The spatial transformations of the three types of bursts are shown in Fig. 6. It can be observed that $F[k]$ is zero in Fig. 6a, corresponding to the constant burst type in Fig. 5a, whereas $F[k]$ in Fig. 6c exhibits a peak with a maximum of approximately 0.4, reflecting the quasi-periodic burst type in Fig. 5c, and $F[k]$ is randomly distributed in Fig. 6b, indicating the non-periodic type in Fig. 5b. The three types of $F[k]$ distributions correspond to the three bursting modes of brain regions that are stable, chaotic, or periodic.

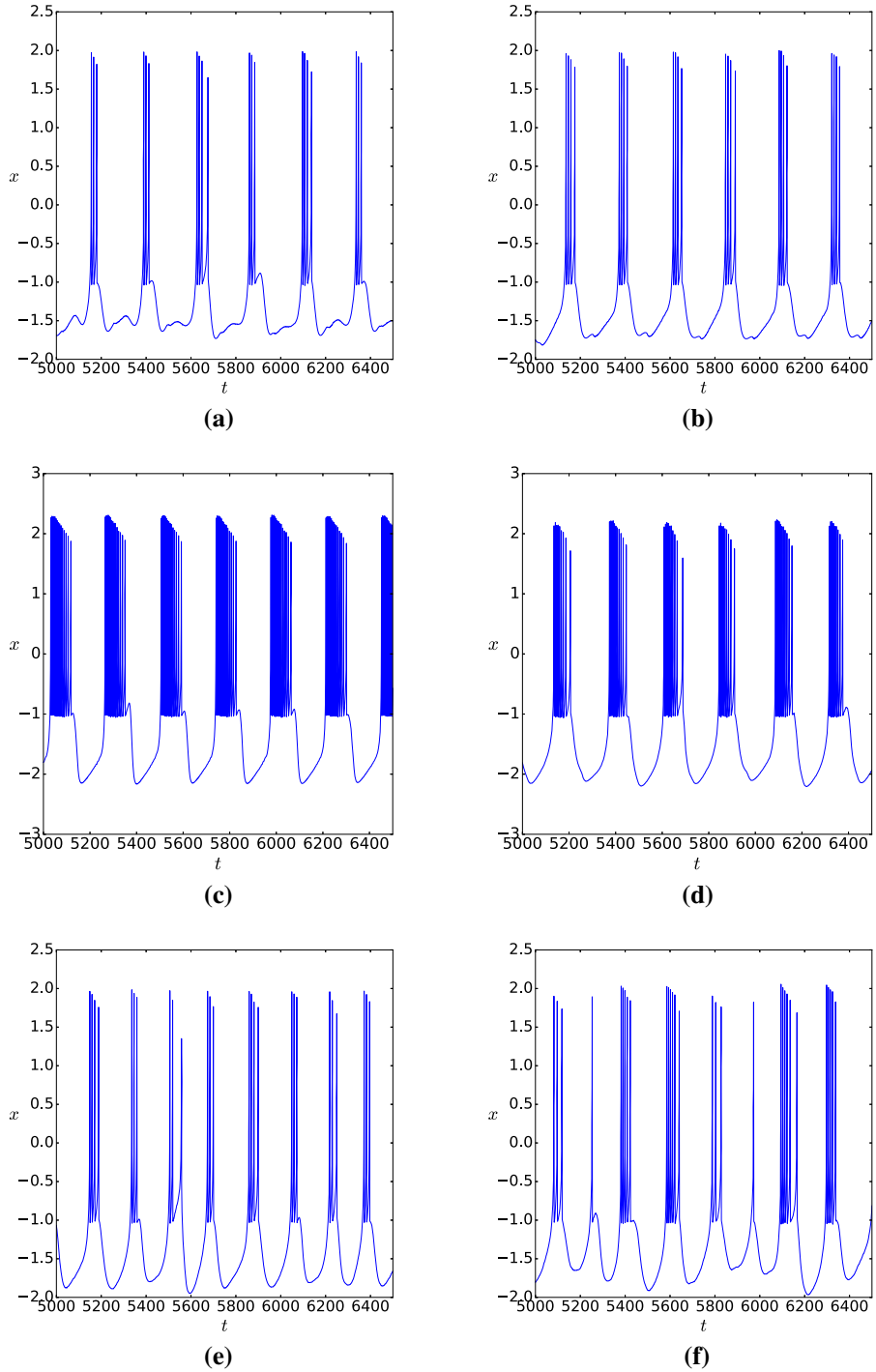

Fig. 4 Time evolution of x for different brain regions in the functional brain network of subject No. 9. **a** Right amygdala (AMYG, R). **b** Left angular gyrus (ANG, L). **c** Right orbitofrontal cortex (inferior) (ORBinf, R). **d** Right posterior cingulate cortex (PCC, R). **e** Right cuneus (CUN, R). **f** Right precentral gyrus (PreCG, R)

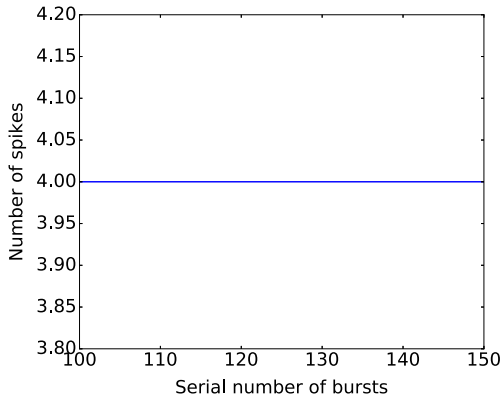

(a)

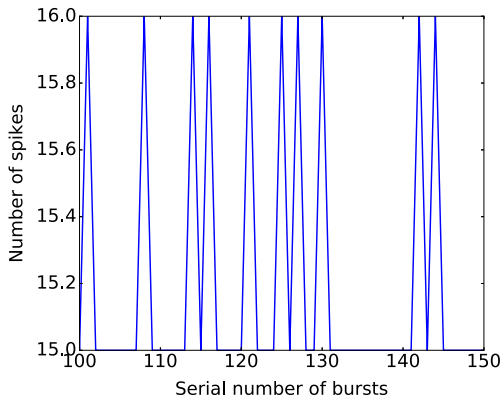

(b)

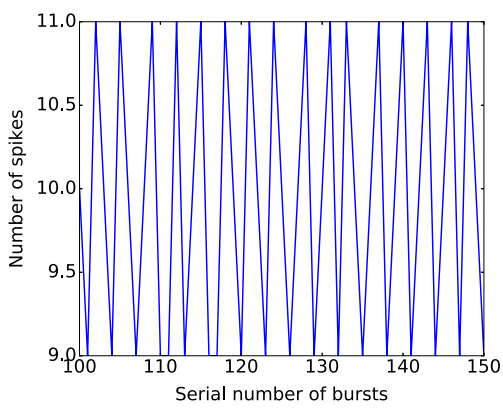

(c)

Fig. 5 Spike numbers in bursts. **a** Right angular gyrus (ANG, R), stable value. **b** Left inferior frontal gyrus (triangular) (IFGtriang, L), non-periodic evolution. **c** Left cuneus (CUN, L), periodic evolution. All nodes have the same parameters described in Sect. 4.1

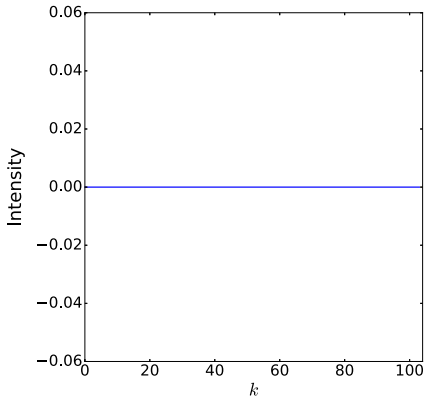

(a)

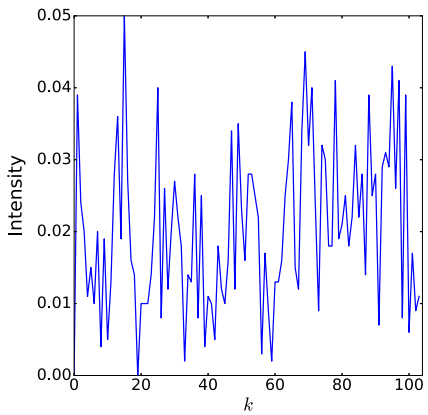

(b)

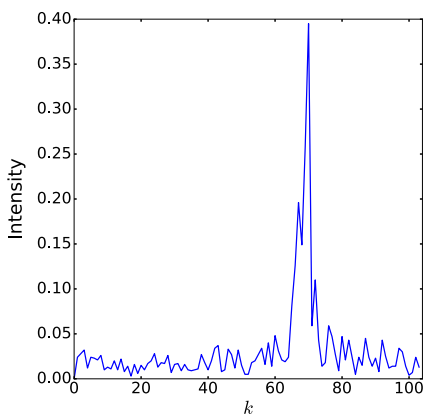

(c)

Fig. 6 Distribution of number evolution after spatial transformation. **a** Right angular gyrus (ANG, R), stable value. **b** Left Inferior frontal gyrus (triangular) (IFGtriang, L), non-periodic evolution. **c** Left cuneus (CUN, L), periodic evolution

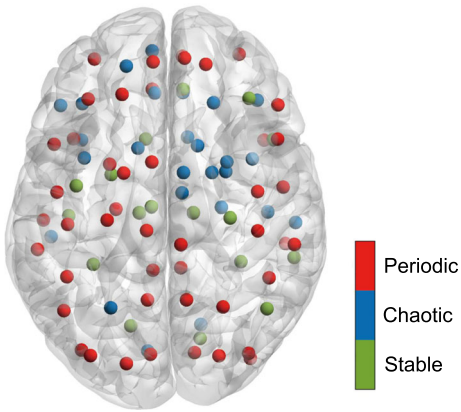

Fig. 7 Bursting modes of brain regions in the subject No. 9 (axial views). Red indicates periodic bursting, blue indicates chaotic bursting, and green indicates stable bursting. The figure is plotted with BrainNet Viewer [31]

The bursting modes of the brain regions were susceptible to the initial values. To eliminate the dependence of the initial values, 200 repeated simulations were performed with different initial values. Therefore, the statistical stability of the output states of the network was ensured. We classified the bursting mode types of the brain regions according to a standard. If the probability of the periodic bursting mode or stable bursting mode appearing in a brain region was more than 50%, then the bursting mode of the brain region was considered to be periodic or stable, respectively. Otherwise, it was considered a chaotic bursting mode. The bursting modes of all brain regions in subject No. 9 are shown in Fig. 7. We found that the dynamic states of the left and right hemispheres of the subject were asymmetric, consistent with the known asymmetric function of the left and right brain hemispheres.

4.2 Homogeneity of functional brain networks for 15 subjects

We investigated the dynamics of the brain regions of the functional brain networks in 15 subjects using the same method and found that the dynamic characteristics of brain regions were basically consistent with those of subject No. 9. In other words, there are three types of bursting modes in the functional brain network, as shown in Fig. 6.

4.2.1 Communication capabilities of bursting modes

The dynamic modes of brain regions vary under different circumstances. For a neural system proceeding from a resting state to a working mode, its dynamics will go from chaotic to cyclical [32]. Therefore, the dynamics of brain regions play a very important role in the transmission and processing of information. To determine which of the three bursting modes represents the active mode of brain regions in the resting state, it is necessary to analyze and compare the communication capabilities of the three bursting modes. External regular signals were added to the nodes of networks to explore the communication capabilities of different modes, as Pariz et al. did [33]. A sinusoidal signal was added to all nodes of the network, as described in Eq. (6)

$$\begin{aligned} \dot{x}_i &= y_i - ax_i^3 + bx_i^2 - z_i + I_{\text{bias}} + I_{ext} \\ &\quad + \tfrac{\sigma}{90}\textstyle\sum_{j=1}^{90} W_{ij}x_j \\ \dot{y}_i &= c - dx_i^2 - y_i + \tfrac{\sigma}{90}\textstyle\sum_{j=1}^{90} W_{ij}y_j \\ \dot{z}_i &= r\,[s(x_i - x_r) - z_i] \\ I_{ext} &= 40 \times 1.2 \times sin(2\pi t/cycle) \end{aligned} \quad , \tag{6}$$

where I_{ext} is the external stimulus signal. All parameters used in the equation are the same as those in Sect. 4.1. To eliminate the interference caused by different initial conditions, we set the initial values of x_i, y_i, and z_i to 0. Figure 8a shows the spontaneous outputs of a brain region without external input, whereas Fig. 8b shows the outputs of the brain region with the sinusoidal signal added. Next, we performed a Fourier transform on the outputs of the brain regions with and without the sinusoidal signal added. Figure 8c and d shows the cycle spectrum of brain regions with and without an external stimulus signal. The response intensity of the sinusoidal signal in the cycle spectrum was used to characterize the communication capability of the brain. Figure 9 shows the average response strength of the three modes in the functional networks of the 15 subjects with different cycles. In most cases, the response intensities of both the stable and periodic modes were almost the same and stronger than those of the chaotic modes. In addition, we noticed that the non-periodic modes of many brain regions were transformed into periodic modes when the sinusoidal stimulus was added, which means that the periodic mode is an active state.

Although the above method can intuitively provide the communication capabilities of different bursting

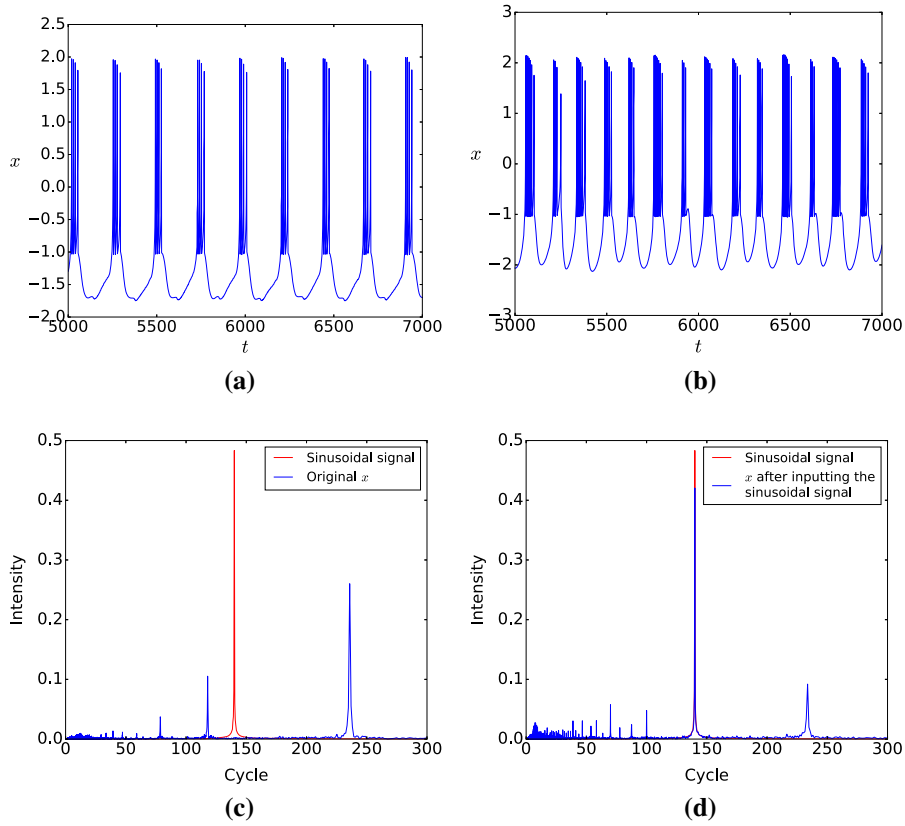

Fig. 8 **a** and **b** show the outputs of the right angular gyrus (ANG, R) of subject No. 9 before and after the sinusoidal signal is added. With the addition of sinusoidal signals, the dynamics of the brain region were more abundant. **c** Cycle spectrum without sinusoidal stimulation. **d** Spectrum distribution with added sinusoidal stimulation. We performed a Fourier transform on the brain region outputs in time t of the Hindmarsh–Rose (HR) model. Because the unit of t has not been set in the HR model, the intensities of the Fourier transform of brain region outputs are expressed in cycles. The frequency is proportional to the inverse of the cycle

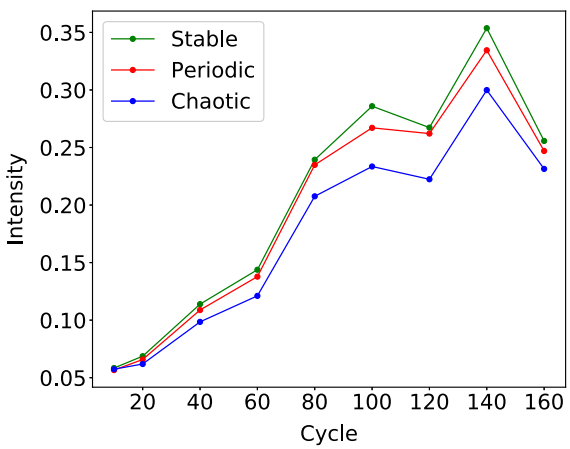

Fig. 9 The average response intensity of three modes of 15 subjects. Stable mode and periodic mode have similar response intensity in different cycles. The response strength of the chaotic mode is the weakest

modes, there is still a shortcoming. We used functional brain networks of the resting state as the connection structures of the networks used. This means that the subjects did not perform any specific tasks when the functional correlation information was measured. Regular external stimuli should not be added to resting brain networks. Otherwise, they will go against the initial conditions of the experiment. To avoid this, we introduced a state space to analyze and compare the communication capabilities of the three bursting modes.

4.2.2 State space

The two-dimensional state space is formed by the average time width of bursts and the average spike number of bursts. It can be used to describe the communication behavior between neuron populations [30]. We first explored the feasibility of analyzing the dynamics of functional brain networks using the state-space method. In our model, increasing bias current I_{bias} and gain coefficients σ correspond to increasing excitability and connection strength, respectively. We simulated the dynamic behaviors of the functional brain networks of 15 subjects under different bias currents I_{bias} and different gain coefficients σ. The remaining parameters were

the same as those described in Sect. 4.1. Considering that the final state of the networks is susceptible to the initial values, repeating simulations were performed to ensure statistical stability for the network output states. The state distributions of all brain regions for 15 subjects at different I_{bias} values in the state space are shown in Fig. 10a. A resting brain network is thought to be in the critical state of multiple modes to quickly respond to external stimulations [34,35]. Therefore, the fitting curves of the distributions can be used as the separatrixes of the state space. Figure 10b shows the fitting curves at different I_{bias} values. The space is divided into two areas based on fitting curves, such as threshold curve. When the state of a brain region is above the separatrix in the state space, the output of the brain region can be effectively responded and transmitted among brain regions. Otherwise, it cannot be delivered effectively. We define the area above the separatrix as a communicable area and that below as a non-communicable area. Therefore, the size of the communicable area represents the strength of the communication capabilities. The position of the separatrix is related to the dynamics of the neural network and its connection structure. Enhancing excitability and synaptic weights can improve the communication capability [30]. As shown in Fig. 10b, as the I_{bias} increases, the fitting lines gradually move down and right, indicating that the information transmission capabilities of networks become stronger. The state distribution of the brain regions in the state space under different gain coefficients σ is shown in Fig. 10c. As the gain coefficient σ increases, the spontaneous signals of the brain regions are more widely distributed in the state space, showing stronger communication capabilities. The results are identical to the theory proposed by Hahn et al. [30], indicating that the state-space method is feasible in our model.

We then used the state-space method to identify the communication capabilities of different bursting modes. The state distributions of the different bursting modes in the state space are shown in Fig. 11a–c. The dynamic parameters in the networks of the 15 subjects were the same as those in Sect. 4.1. Observing the state distributions of different dynamic modes in the state space, one can find a stepwise state distribution of the stable mode, whereas the distributions of the other modes are relatively random. We speculate that brain regions in stable modes transmit signals only in critical states, but not in active states. The fitting curves of the different bursting modes are plotted in

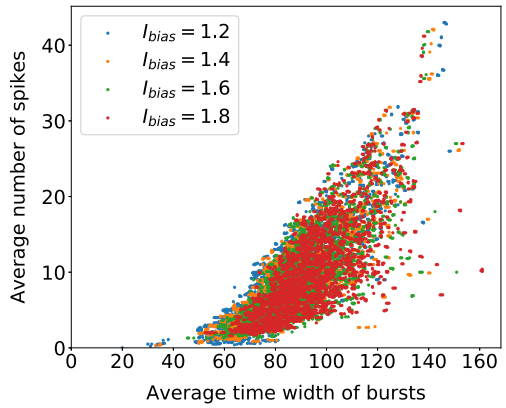

(a)

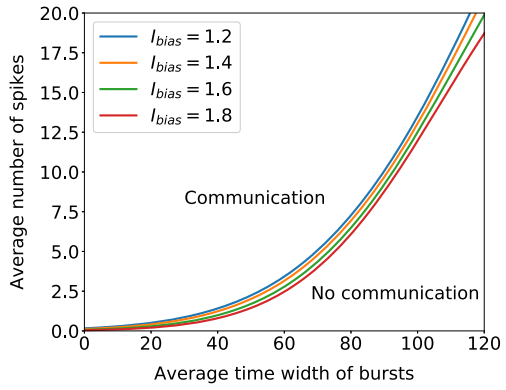

(b)

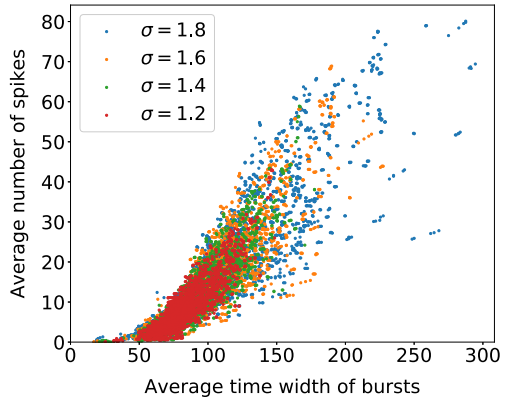

(c)

Fig. 10 The spontaneous signal distributions of brain regions for 15 subjects in the state space under different parameters. In order to obtain sufficient data, each parameter is repeated four times. **a** $\sigma = 1.2$, different I_{bias}. **b** $\sigma = 1.2$, fitting curves of different I_{bias} in state space. **c** $I_{\text{bias}} = 1.2$, different gain coefficients σ

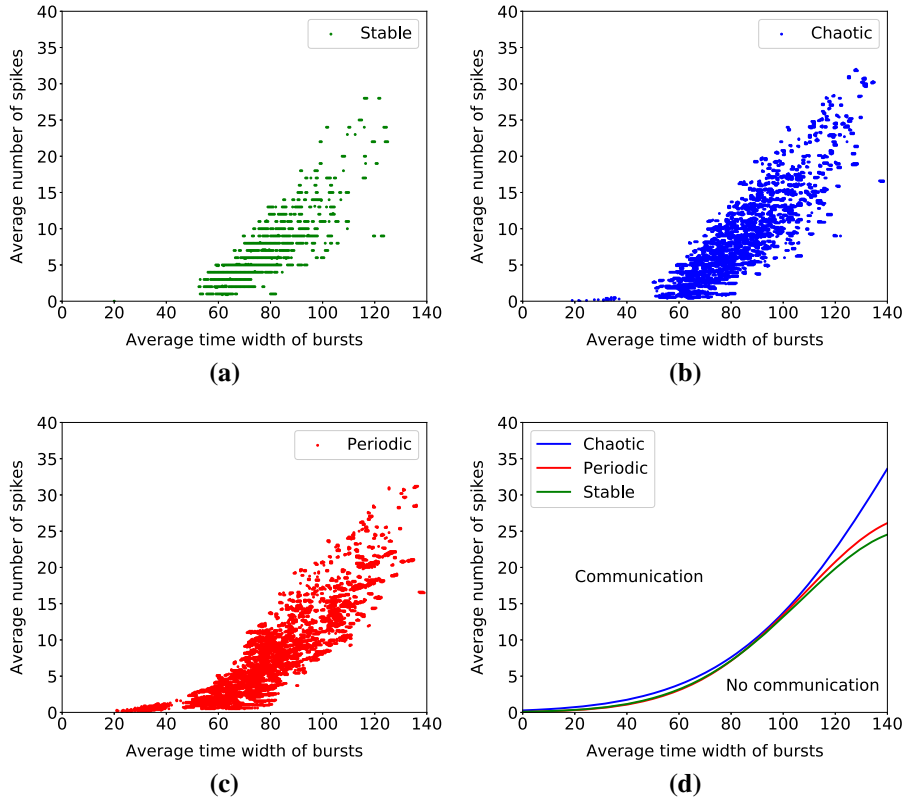

Fig. 11 The spontaneous signal distributions of brain regions with different modes in the state space. **a** Stable mode. **b** Chaotic mode. **c** Periodic mode. **d** Fitting curves of the three dynamic modes in the state space. Data are obtained from functional brain networks of 15 subjects by repeating 200 times

Fig. 11d. The red curve representing the periodic mode is located on the right side of the blue curve representing the chaotic mode, meaning that the periodic mode has a larger communicable area in the state space than that of the chaotic mode. When a brain region periodically oscillates, resonance can provide a new communication mode between brain regions so that a weaker signal can also be successfully transmitted [30,36]. In summary, we consider that the brain regions with a periodic mode are active. The results of the communication capabilities of different bursting modes using the state-space method are identical to those of the response to external regular signals.

4.2.3 Bursting mode distribution in the brain

We performed a statistical analysis of the bursting mode distribution in the brains of 15 subjects. The results are shown in Fig. 12. We found some differences in bursting mode distributions in the brain regions of the 15 subjects. To reveal similarities among all subjects, we counted the frequency of all bursting modes in all brain regions in all subjects. The results are shown in Fig. 13. There are 12 brain regions, namely the left and right posterior cingulate cortex (PCC, L & R), right superior frontal cortex (medial orbital) (ORBsupmed, R), left parahippocampal cortex (PHC, L), left inferior parietal lobule (IPL, L), right inferior temporal gyrus (ITG, R), left middle temporal gyrus (MTG, L), left cuneus (CUN , L), left inferior frontal gyrus (opercular) (IFGoperc, L), right inferior frontal gyrus (triangular) (IFGtriang, R), left paracentral lobule (PCL, L), and left inferior occipital gyrus (IOG, L), with a common active status; that is, those brain regions in at least 7 of the 15 subjects that exhibit periodic bursting modes.

5 Discussion

To date, many studies have focused on functional brain networks in the resting state. In 1997, Shulman et al. first discovered that the activity of certain specific cerebral cortices decreased when subjects performed tasks [37]. Subsequently, Raichle et al. used PET to show that these brain regions with reduced activity during task performance show stronger excitability than

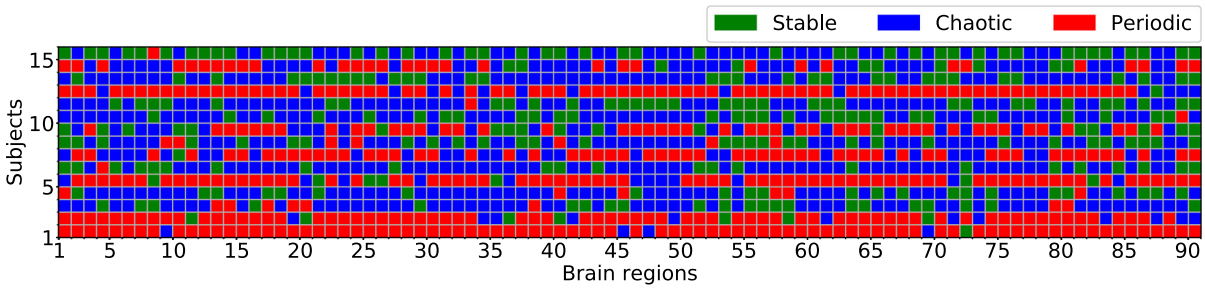

Fig. 12 Dynamic mode of all brain regions in 15 subjects

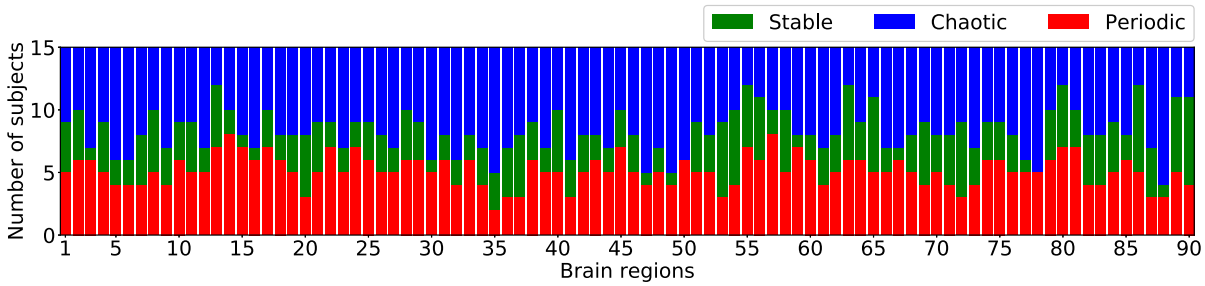

Fig. 13 Number of subjects with the same mode in 90 brain regions. The abscissa indicates the brain region, and the ordinate the number of subjects of the mode

other regions, indicating an organizational activity in the brain resting state [38], rather than at complete rest. The network of brain regions participating in this self-organizing activity is called the default mode network (DMN). Since then, many studies related to DMN have been reported. These studies were carried out in different ways, such as task-driven, disease state–DMN relationships, functional connectivity processes, self-referential processing and mind-wandering, neurophysiology, and cell biology [39]. The default brain network in the resting state is mainly composed of the ventral medial prefrontal cortex (VMPC), dorsal medial prefrontal cortex (DMPC), PCC, and hippocampal formation (HF, including the entorhinal cortex and surrounding cortex, e.g., PHC, IPL, lateral temporal cortex (LTC), and other core brain regions) [40].

The PCC and the medial precuneus are prominent areas of the DMN and were the first to come to attention [39]. In our study, the PCC (L & R) were activated (periodic mode) in the functional brain networks of most subjects, consistent with previous studies on the DMN. The HF and PHC form a subsystem of the default brain network, which is closely connected to the PCC [40]. Our results showed that the PHC (L) of eight subjects was in the periodic mode.

The VMPC is a key area of the default brain network. It receives and transmits external information to the hypothalamus, amygdala, and other structures via the orbital frontal cortex [39]. The default brain network with VMPC as a core node participates in social behavior and emotional control, which are the main causes of individual personality. In our study, ORBsupmed (R), a brain region with a relatively high consistency of periodic mode in all subjects, was located exactly in the VMPC, which is the key node of information transmission.

The DMPC is another key area of the DMN, which is related to self-referential judgments [39]. When DMPC activity increases, VMPC activity decreases, which is consistent with the need to reduce the impact of emotions during tasks. Interestingly, in our results, IFGoperc (L) and IFGtriang (R), two highly consistent periodic-patterned brain regions, were located near the DMPC.

Among the remaining active brain regions, the CUN (L) is located near the precuneus, whereas the PCL (L) is located at the junction of the frontal lobe and the parietal lobes, near the DMN components. In addition, the LTC is an integral part of the DMN. Hagmann et al. found a structural core within the posterior medial and parietal cerebral cortex through DSI [41]. The structural core contains brain regions that form the posterior components of the human DMN . Buckner et al. found that the low metabolic pattern of patients with AD was

located in the posterior DMN components, including the LTC and IPL [42]. Among the periodic brain regions with high consistency in our results, the ITG (R) and MTG (L) belong to the LTC. In addition, the IPL (L) in most functional brain networks constructed in this study also showed an active state.

In summary, among the 12 active brain regions obtained from the dynamic simulation of the resting brain, all but the IOG (L) were DMN components or near brain regions related to the DMN. These results are consistent with real brain activity in the resting state.

6 Conclusion

Here, we propose a method based on functional brain networks and an HR neural network model to explore brain dynamics. In this method, a functional brain network was constructed according to resting-state fMRI data. An HR neuron was used as a node in place of a brain region in a functional brain network, and Pearson correlations as the synapse weight. A dynamic model of the functional brain network was established. The dynamics of the functional brain network were investigated using the dynamic model. Simulation results revealed that the activity of brain regions released spike bursts, which could be classified into three modes: periodic, chaotic, or stable. A state-space method was employed to analyze the dynamic characteristics of brain regions. We found that the periodic bursting mode had stronger communication capabilities than the chaotic bursting mode and verified that the dynamic activities of the left and right hemispheres were asymmetric. We analyzed the bursting modes of brain regions of all subjects and found 12 brain regions in periodic bursting modes with high consistency in all subjects. Most of these brain regions fell into or near the active area of the DMN. Our results prove that the proposed method is suitable for investigating the dynamics of functional brain networks.

Acknowledgements This work was supported by the Natural Science Foundation of China (Grant No. 31270026).

Declarations

Conflict of interest The authors declare that they have no conflict of interest.

Ethical approval This study was approved by the research ethics review board of Zhejiang University in China and was conducted in accordance with the guidelines of Helsinki Declaration.

References

1. Eliasmith, Chris, Stewart, Terrence C., Choo, Xuan, Bekolay, Trevor, DeWolf, Travis, Tang, Yichuan, Rasmussen, Daniel: A large-scale model of the functioning brain. Science **338**(6111), 1202–1205 (2012)
2. George, Dileep, Hawkins, Jeff: Towards a mathematical theory of cortical micro-circuits. PLoS Comput. Biol. **5**(10), e1000532 (2009)
3. Riesenhuber, Maximilian, Tomaso, Poggio: Hierarchical models of object recognition in cortex. Nat. Neurosci. **2**(11), 1019–1025 (1999)
4. Rivest, Françcois, Bengio, Yoshua, Kalaska, John: Brain inspired reinforcement learning. Adv. Neural Inf. Process. Syst. **17**, 1129–1136 (2004)
5. Serre, Thomas, Oliva, Aude, Poggio, Tomaso: A feedforward architecture accounts for rapid categorization. Proc. Natl. Acad. Sci. **104**(15), 6424–6429 (2007)
6. Insel, Thomas R., Landis, Story C.: Twenty-five years of progress: the view from nimh and ninds. Neuron **80**(3), 561–567 (2013)
7. Siettos, Constantinos: Starke, Jens: Multiscale modeling of brain dynamics: from single neurons and networks to mathematical tools. Wiley Interdisciplinary Reviews: Systems Biology and Medicine **8**(5), 438–458 (2016)
8. Hodgkin, Alan L., Huxley, Andrew F.: A quantitative description of membrane current and its application to conduction and excitation in nerve. J. Physiol. **117**(4), 500–544 (1952)
9. FitzHugh, Richard: Mathematical models of threshold phenomena in the nerve membrane. Bull. Math. Biophys. **17**(4), 257–278 (1955)
10. Jinichi, Nagumo, Suguru, Arimoto, Shuji, Yoshizawa: An active pulse transmission line simulating nerve axon. Proc. IRE **50**(10), 2061–2070 (1962)
11. Rössler, Otto E.: An equation for continuous chaos. Phys. Lett. A **57**(5), 397–398 (1976)
12. Rössler, Otto E.: An equation for hyperchaos. Phys. Lett. A **71**(2–3), 155–157 (1979)
13. Hindmarsh, James L., Rose, R.M.: A model of neuronal bursting using three coupled first order differential equations. Proceedings of the Royal society of London. Series B. Biological sciences **221**(1222), 87–102 (1984)
14. Ying, Xu, Yeye, Guo, Guodong, Ren, Jun, Ma.: Dynamics and stochastic resonance in a thermosensitive neuron. Appl. Math. Comput. **385**, 125427 (2020)
15. Ying, Xu, Minghua, Liu, Zhigang, Zhu, Jun, Ma.: Dynamics and coherence resonance in a thermosensitive neuron driven by photocurrent. Chin. Phys. B **29**(9), 098704 (2020)
16. Baptista, M.S., Kakmeni, F.M., Grebogi, Celso: Combined effect of chemical and electrical synapses in Hindmarsh-Rose neural networks on synchronization and the rate of information. Phys. Rev. E **82**(3), 036203 (2010)
17. Hizanidis, Johanne, Kanas, Vasileios G., Bezerianos, Anastasios, Bountis, Tassos: Chimera states in networks of nonlo-

cally coupled Hindmarsh-Rose neuron models. Int. J. Bifurc. Chaos **24**(03), 1450030 (2014)
18. Rattenborg, N.C., Amlaner, C.J., Lima, S.L.: Behavioral, neurophysiological and evolutionary perspectives on unihemispheric sleep. Neurosci. Biobehav. Rev. **24**(8), 817–842 (2000)
19. Malik, S.A., Mir, A.H.: Synchronization of hindmarsh rose neurons. Neural Netw. **123**, 372–380 (2020)
20. Bassett, D.S., Meyer-Lindenberg, A.S., Achard, S., Duke, T., Bullmore, E.: Adaptive reconfiguration of fractal small-world human brain functional networks. Proc. Natl. Aad. Sci. **103**(51), 19518–19523 (2006)
21. Supekar, Kaustubh, Menon, Vinod, Rubin, Daniel, Musen, Mark, Greicius, Michael D.: Network analysis of intrinsic functional brain connectivity in alzheimer's disease. PLoS Comput. iol. **4**(6), e1000100 (2008)
22. Meng, Liang, Yuan, Zhou, Tianzi, Jiang, Zhening, Liu, Lixia, Tian, Haihong, Liu, Yihui, Hao: Widespread functional disconnectivity in schizophrenia with resting-state functional magnetic resonance imaging. Neuroreport **17**(2), 209–213 (2006)
23. Micheloyannis, S., Pachou, E., Stam, C.J., Breakspear, M., Bitsios, P., Vourkas, M., Erimaki, S., Zervakis, M.: Small-world networks and disturbed functional connectivity in schizophrenia. Schizophr. Res. **87**(1–3), 60–66 (2006)
24. Santos, M.S., Szezech, J.D., Borges, F.S., Iarosz, K.C., Caldas, I.L., Batista, A.M., Viana, R.L., Kurths, J.: Chimera-like states in a neuronal network model of the cat brain. Chaos, Solitons & Fractals **101**, 86–91 (2017)
25. Ling, Kang, Changhai, Tian, Siyu, Huo, Zonghua, Liu: A two-layered brain network model and its chimera state. Sci. Rep. **9**(1), 1–12 (2019)
26. Pariz, Aref, Esfahani, Zahra G., Parsi, Shervin S., Valizadeh, Alireza, Canals, Santiago, Mirasso, Claudio R.: High frequency neurons determine effective connectivity in neuronal networks. NeuroImage **166**, 349–359 (2018)
27. Ziaeemehr, Abolfazl, Zarei, Mina, Valizadeh, Alireza, Mirasso, Claudio R.: Frequency-dependent organization of the brain's functional network through delayed-interactions. Neural Netw. **132**, 155–165 (2020)
28. Fox, Michael D., Raichle, Marcus E.: Spontaneous fluctuations in brain activity observed with functional magnetic resonance imaging. Nat. Rev. Neurosci. **8**(9), 700–711 (2007)
29. Koch, Martin A., Norris, David G., Hund-Georgiadis, Margret: An investigation of functional and anatomical connectivity using magnetic resonance imaging. Neuroimage **16**(1), 241–250 (2002)
30. Gerald, Hahn, Adrian, Ponce-Alvarez, Gustavo, Deco, Aertsen, A.D., Kumar, Arvind: Portraits of communication in neuronal networks. Nat. Rev. Neurosci. **20**(2), 117–127 (2019)
31. Mingrui, Xia, Jinhui, Wang, Yong, He: Brainnet viewer: a network visualization tool for human brain connectomics. PloS one **8**(7), e68910 (2013)
32. Skarda, Christine A., Freeman, Walter J.: How brains make chaos in order to make sense of the world. Behav. Brain Sci. **10**(2), 161–173 (1987)
33. Pariz, Aref, Fischer, Ingo, Valizadeh, Alireza, Mirasso, Claudio R: Transmission delays and frequency detuning can regulate information flow between brain regions. *bioRxiv*, page 2020.07.09.194969, (2020)
34. Petermann, T., Thiagarajan, T.C., Lebedev, M.A., Nicolelis, M.A.L., Chialvo, D.R., Plenz, D.: Spontaneous cortical activity in awake monkeys composed of neuronal avalanches. Proc. Natl. Acad. Sci. **106**(37), 15921–15926 (2009)
35. Azouz, Rony, Gray, Charles M.: Cellular mechanisms contributing to response variability of cortical neurons in vivo. J. Neurosci. **19**(6), 2209–2223 (1999)
36. Rezaei, H., Aertsen, A., Kumar, A., Valizadeh, A.: Facilitating the propagation of spiking activity in feedforward networks by including feedback. PLoS Comput. Biol. **16**(8), e1008033 (2020)
37. Shulman, G.L., Corbetta, M., Buckner, R.L., Fiez, J.A., Miezin, F.M., Raichle, M.E., Petersen, S.E.: Common blood flow changes across visual tasks: I increases in subcortical structures and cerebellum but not in nonvisual cortex. J. Cognit. Neurosci. **9**(5), 624–647 (1997)
38. Raichle, Marcus E., MacLeod, Ann Mary, Snyder, Abraham Z., Powers, William J., Gusnard, Debra A., Shulman, Gordon L.: A default mode of brain function. Proc. Natl. Acad. Sci. **98**(2), 676–682 (2001)
39. Raichle, Marcus E.: The brain's default mode network. Ann. Rev. Neurosci. **38**, 433–447 (2015)
40. Buckner, Randy L., Andrews-Hanna, Jessica R., Schacter, Daniel L.: The brain's default network: anatomy, function, and relevance to disease. Ann. N. Y. Acad. Sci. **1124**(1), 1–38 (2008)
41. Hagmann, Patric, Cammoun, Leila, Gigandet, Xavier, Meuli, Reto, Honey, Christopher J., Van Wedeen, J., Sporns, Olaf: Mapping the structural core of human cerebral cortex. PLoS Biol. **6**(7), e159 (2008)
42. Buckner, Randy L., Snyder, Abraham Z., Shannon, Benjamin J., LaRossa, Gina, Sachs, Rimmon, Fotenos, Anthony F., Sheline, Yvette I., Klunk, William E., Mathis, Chester A., Morris, John C., et al.: Molecular, structural, and functional characterization of alzheimer's disease: evidence for a relationship between default activity, amyloid, and memory. J. Neurosci. **25**(34), 7709–7717 (2005)